

Evidence for a cysteine-mediated mechanism of excitation energy regulation in a photosynthetic antenna complex

Gregory S. Orf^{a,b,c,1}, Rafael G. Saer^{b,c}, Dariusz M. Niedzwiedzki^c, Hao Zhang^{a,c}, Chelsea L. McIntosh^{b,2}, Jason W. Schultz^a, Liviu M. Mirica^a, and Robert E. Blankenship^{a,b,c,3}

^aDepartment of Chemistry, Washington University in St. Louis, St. Louis, MO 63130; ^bDepartment of Biology, Washington University in St. Louis, St. Louis, MO 63130; and ^cPhotosynthetic Antenna Research Center, Washington University in St. Louis, St. Louis, MO 63130

Edited by Brian W. Matthews, University of Oregon, Eugene, OR, and approved May 26, 2016 (received for review March 2, 2016)

Light-harvesting antenna complexes not only aid in the capture of solar energy for photosynthesis, but regulate the quantity of transferred energy as well. Light-harvesting regulation is important for protecting reaction center complexes from overexcitation, generation of reactive oxygen species, and metabolic overload. Usually, this regulation is controlled by the association of light-harvesting antennas with accessory quenchers such as carotenoids. One antenna complex, the Fenna–Matthews–Olson (FMO) antenna protein from green sulfur bacteria, completely lacks carotenoids and other known accessory quenchers. Nonetheless, the FMO protein is able to quench energy transfer in aerobic conditions effectively, indicating a previously unidentified type of regulatory mechanism. Through de novo sequencing MS, chemical modification, and mutagenesis, we have pinpointed the source of the quenching action to cysteine residues (Cys49 and Cys353) situated near two low-energy bacteriochlorophylls in the FMO protein from *Chlorobaculum tepidum*. Removal of these cysteines (particularly removal of the completely conserved Cys353) through *N*-ethylmaleimide modification or mutagenesis to alanine abolishes the aerobic quenching effect. Electrochemical analysis and electron paramagnetic resonance spectra suggest that in aerobic conditions the cysteine thiols are converted to thiyl radicals which then are capable of quenching bacteriochlorophyll excited states through electron transfer photochemistry. This simple mechanism has implications for the design of bio-inspired light-harvesting antennas and the redesign of natural photosynthetic systems.

photosynthesis | Fenna–Matthews–Olson protein | excitation quenching | thiyl radical | light-harvesting

Photosynthesis can be performed in the presence of oxygen (oxygenic photosynthesis, in which water is the electron source) or in its absence (anoxygenic photosynthesis, in which other reduced species such as sulfide are the electron sources) (1–3). Many bacteria performing anoxygenic photosynthesis contain type I reaction center (RC) protein complexes that use Fe-S clusters to transfer electrons to ferredoxin or related molecules after photoinduced charge separation (4–6). These Fe-S clusters are easily damaged by molecular oxygen. Therefore, anoxygenic phototrophs must use a pathway either to remove oxygen or to reduce the rate of photosynthesis whenever oxygen is encountered (1, 5).

Phototrophic members of the bacterial phylum Chlorobi (green sulfur bacteria, GSBs) are anoxygenic phototrophs that contain such a type I RC. They also contain two peripheral antenna complexes that aid in regulating light absorption and energy transfer: the chlorosome and the homotrimeric Fenna–Matthews–Olson (FMO) protein complex. When oxygen is encountered, the bacteria are able to decrease the output of photosynthesis. This process involves creating trapping sites in the antenna complexes where de-excitation processes outcompete the rate of energy transfer to the RC, preventing RC damage. This process is well understood in the chlorosome, involving redox-sensitive quinones dispersed among the self-assembled bacteriochlorophyll (BChl) pigments (7–10). The

photoprotective mechanism in the FMO protein, in contrast, has thus far been enigmatic.

Studies in the 1980s and 1990s first described a “dithionite effect,” in which adding the strong reductant sodium dithionite [midpoint potential vs. natural hydrogen electrode (NHE) approximately -400 mV] to an oxygenated solution of FMO increases the fluorescence emission response and lengthens the dominant fluorescence lifetime of the complex’s BChl *a* pigments (11, 12). In oxidizing conditions, the fast lifetime of the quenching pathway (60 ps) is thought to compete with the rate of energy transfer to the RC. This pathway effectively disappears in reducing conditions, allowing the pigments to fluoresce with lifetimes similar to that of monomeric BChl *a* (2 ns) (13). It was suggested that the quenching effect might be controlled by a modified aromatic amino acid (e.g., tyrosylquinone or tryptophylquinone) that plays a role similar to that of the excitation-quenching quinones found in the chlorosome (12). However, to this point, no such amino acid has been found via crystallography or other methods.

The goals of this study were to describe the molecular source of this redox-sensing effect, determine the midpoint potential of the redox-sensing species, and establish a viable excitation-quenching mechanism based on the results. We discovered that

Significance

All photosynthetic organisms face the challenge of absorbing solar energy and regulating its flow through their light-harvesting antennas across widely varying photic conditions. For anoxygenic phototrophs, this process is complicated by the need to down-regulate photosynthetic output when oxygen is encountered. The Fenna–Matthews–Olson protein from green sulfur bacteria is able to quench excitations in aerobic conditions effectively despite its apparent lack of photoprotective accessory molecules, indicating a previously unidentified type of energy transfer regulation. In this study, we provide evidence for a novel energy-quenching mechanism involving cysteine–bacteriochlorophyll photochemistry. This interaction should be able to be programmed into other natural or bio-inspired antennas, opening new possibilities for regulating these systems in response to excess light.

Author contributions: G.S.O. and R.E.B. designed research; G.S.O., R.G.S., D.M.N., H.Z., C.L.M., J.W.S., and L.M.M. performed research; G.S.O., R.G.S., D.M.N., and H.Z. analyzed data; and G.S.O. and R.E.B. wrote the paper.

The authors declare no conflict of interest.

This article is a PNAS Direct Submission.

See Commentary on page 8562.

¹Present address: Center for Bioenergy and Photosynthesis, School of Molecular Sciences, Arizona State University, Tempe, AZ 85281.

²Present address: Department of Poly Science and Math, College of Letters and Sciences, Arizona State University at Downtown Phoenix, Phoenix, AZ 85004.

³To whom correspondence should be addressed. Email: blankenship@wustl.edu.

This article contains supporting information online at www.pnas.org/lookup/suppl/doi:10.1073/pnas.1603330113/-DCSupplemental.

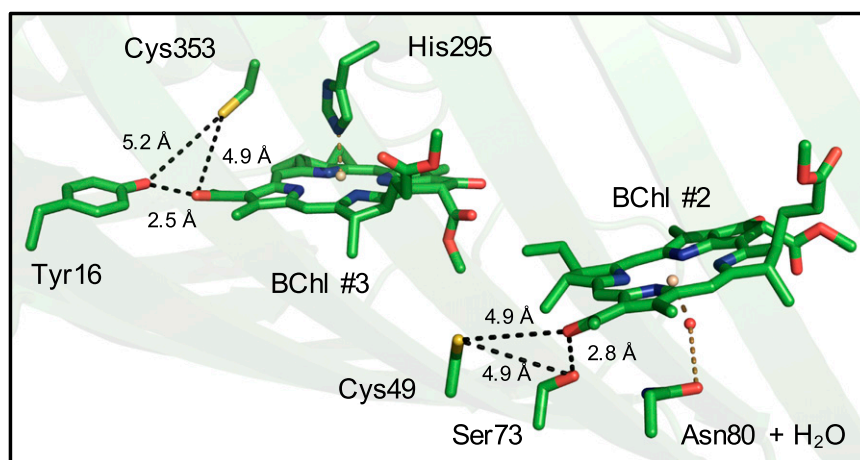


Fig. 1. Crystal structure of the FMO protein from *Cba. tepidum* (PDB code 3ENI, visualized in PyMOL), highlighting the cysteine residues of interest and their proximity to BChl *a* 2 and 3 in a single protein monomer. BChl *a* phytol tails are omitted for clarity. Black dotted lines are labeled with interatomic distances of interest. Brown dotted lines represent protein-to-pigment coordination bonds.

the two cysteine residues (C49 and C353) in each FMO protein from the model organism *Chlorobaculum (Cba.) tepidum* TLS were highly sensitive to redox conditions. These residues are situated near BChls 2 and 3, the lowest-energy BChls in the complex, but are spatially separated from each other by >20 Å, precluding disulfide bond formation. Chemical modification of these cysteines in vitro substantially changed the energy-transfer profile and the redox modulation of the complex. Producing cysteine-deficient mutants of the protein (14) allowed further evaluation of the quenching effect. A double mutation (C49A/C353A) produced a protein lacking the redox effect altogether. We characterized these changes by using absorption spectroscopy, steady-state and time-resolved fluorescence (TRF) spectroscopy, direct electrochemistry, and electron paramagnetic resonance (EPR) spectroscopy. We propose a mechanism in which the charge state of the cysteines (thiyl radical vs. thiol, dictated by redox conditions) affects the photophysical behavior of the BChl *a* pigments.

Results

Identification of Cysteines as Residues of Interest. In the paper first describing the FMO protein's redox-dependent quenching effect in detail (12), it was suggested that an aromatic amino acid residing near a BChl *a* in the interior of the protein may be modified into a photoactive quinone-like species capable of quenching a BChl *a* excited state. Crystallographic evidence of air-oxidized FMO protein collected since that time does not support this hypothesis (15, 16). Modern MS techniques have the ability to identify modifications at the residue level (17), allowing us to reevaluate the presence or absence of modified amino acids in the FMO protein. Software such as PEAKS (18) allows de novo peptide sequencing, which searches for peptide modifications that may be missed by referencing online peptide databases.

We prepared the FMO protein for LC-MS/MS in two environments. In the aerobic sample, protein precipitation, proteolytic digestion, and peptide purification were performed in open air. In the anaerobic sample, these steps were repeated in an anaerobic chamber with deoxygenated solutions and with the addition of the reductant sodium dithionite to 10 mM. Subsequent peptide mapping indicated that nearly every amino acid in the protein existed in the same, unmodified form equally across both aerobically and anaerobically prepared samples. The only amino acids that showed significant changes were the two cysteine residues Cys49 and Cys353. These cysteines were found to contain more oxidative modifications (i.e., additions of oxygen

atoms to the thiol, resulting in moieties such as cysteic acid) when prepared in aerobic conditions than in anaerobic conditions (Fig. S1). Crystallographic evidence (Fig. 1) shows that Cys49 and Cys353 are within 5 Å of the C-3 acetyl groups of BChls 2 and 3, respectively, and are too separated spatially to form a disulfide bridge (15). BChls 2 and 3 are considered to have two of the lowest pigment-site energies in the complex (19).

Derivatization of Cysteine Residues with *N*-Ethylmaleimide. Although the effect of electrospray ionization in the mass spectrometer on the appearance of these oxidative changes cannot be quantified easily, we decided to assay the role of the cysteines on the protein's redox effect. We covalently maleylated the cysteines using *N*-ethylmaleimide (NEM), which permanently prevents thiol groups from undergoing further redox chemistry (20–22). MS (Figs. S2 and S3) confirmed successful modification of 18.6% of Cys49-containing peptides and 29.3% of Cys353-containing peptides. The low modification efficiency likely results from the limited accessibility of exogenous large molecules to the interior of the protein.

Upon reaction of FMO protein with NEM, changes in the steady-state optical spectra were observed (Fig. 2). Absorption spectra at 298 K (Fig. 2A, *Inset*) showed no change, but at 77 K (Fig. 2A) slight shifts are seen in the Q_y region. Because we believe from MS evidence that 30%, at most, of the cysteines were successfully treated in the NEM-modified sample, then 70% of the sample must be unmodified. We can decompose the NEM-modified protein absorption spectrum into a 100% NEM-modified spectrum by normalizing modified and unmodified spectra and subtracting an NEM-unmodified spectrum scaled at 70% (Fig. 2A, green line). This spectrum shows that the NEM-induced changes primarily affect the spectral region of 795–805 nm. The presence of the maleimide group has likely perturbed the orientation or polarity of the pigment environment corresponding to this region, shifting the site energies to lower energy. The 825-nm band, representing the lowest-energy pigments in the complex and those pigments responsible for steady-state fluorescence, is largely unchanged by NEM modification, indicating that the orientation or polarity of the pigment environment in that region is largely unchanged. Importantly, the increase of fluorescence emission usually seen upon the addition of dithionite is significantly reduced (Fig. 2B) upon NEM modification. Finally, the fluorescence intensity in oxidizing conditions is slightly higher in the NEM-modified protein than in the unmodified protein.

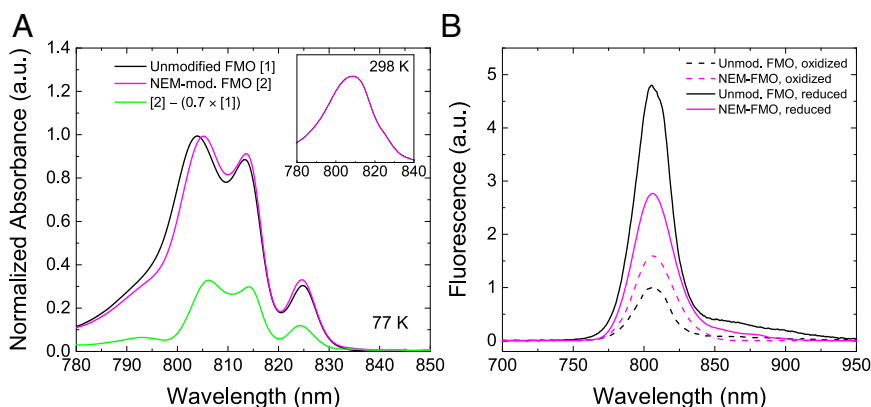


Fig. 2. Optical spectroscopy of NEM-modified and unmodified FMO. (A) 298 K (*Inset*) and 77 K absorption in the Q_y region. Because the success of NEM modification was calculated by MS to be $\sim 30\%$, we subtracted the unmodified FMO absorption spectrum scaled at 70% from that of the NEM-modified FMO spectrum. The resultant plot (green line) estimates the spectrum of a 100% NEM-modified FMO sample. (B) Fluorescence emission (298 K) of NEM-modified and unmodified FMO in air-oxidized and dithionite-reduced conditions.

Steady-State Fluorescence of FMO Cysteine Mutants. To probe further the role of cysteine residues in the fluorescence response of the FMO protein caused by the redox condition, we constructed three site-directed mutants: C49A, C353A, and the double mutant C49A/C353A. We have reported elsewhere (14) a method for genetic engineering of the FMO protein and an in-depth analysis of the absorption changes in the protein upon cysteine mutation. At cryogenic temperature, the absorption spectra of each mutant are subtly different from that of the WT, allowing an in-depth reanalysis of the FMO energetic landscape. An X-ray crystal structure solved for the C49A/C353A double mutant [Protein Data Bank (PDB) ID code 5H8Z] showed that the overall protein structure and pigment orientations are unchanged upon mutation (14). Here we focus on the fluorescence response of the mutants to the addition of dithionite (Fig. 3).

Compared with WT, the C49A mutation alone has no discernible effect on the steady-state fluorescence response upon the addition of dithionite (Fig. 3, *Upper Right*). The C353A mutation (Fig. 3, *Lower Left*) has an intermediate effect: The fluorescence intensity of the reduced form resembles that of the WT and the C49A mutant, but the intensity of the oxidized form is higher than in the WT and C49A mutant. This mutant also shows a distinctive peak splitting not present in the WT. Last, the C49A/C353A double mutant (Fig. 3, *Lower Right*) does not show a fluorescence response that can be attributed to the simple addition of the individual mutations; it shows both intermediate fluorescence intensity and an abolished response to dithionite addition.

TRF. To understand why the steady-state fluorescence spectrum changes so drastically upon NEM modification or cysteine mutation, we performed TRF studies on all protein samples. Because the intensity of steady-state fluorescence is directly linked with the fluorescence decay lifetime (the shorter the lifetime, the less intense the fluorescence), these experiments should clearly demonstrate how the abovementioned mutations/modifications have affected the excited-state properties of the BChls. Representative fluorescence decay traces taken at 815 nm are shown in Fig. 4. Fitting of the traces with a sum of exponential decays, convoluted by the instrument response function (IRF), revealed multiple kinetic components. Their lifetimes and contributions are listed in Table 1.

The oxidized FMO from the C49A mutant and WT demonstrate similar kinetic characteristics of BChl *a* fluorescence decay: a dominating fast kinetic component with a lifetime in the 65–79 ps range (Fig. 4 *A* and *C*). The fluorescence decay traces of the FMO from the C353A and C49A/C353A mutants addi-

tionally show the substantial contribution of a kinetic component with a significantly longer lifetime. Upon dithionite reduction, the FMOs from all the mutants and from WT show essentially the same fluorescence dynamics (Fig. 4 *A* and *D*). Fitting of the decay traces has shown that all mutants gained some new intermediate kinetic component not present in the WT FMO (700–900 ps in C49A and 1.6–1.8 ns in C353A and C49A/C353A). Additionally, in the C353A and C49A/C353A mutants the archetypal long lifetime component [2.0–2.2 ns in the WT (12, 23)] lengthens to 2.6–3.6 ns (Table 1).

Most interestingly, an intermediate, ~ 550 ps kinetic component is present in the NEM-modified FMO (Fig. 4*B*) in both oxidizing and reducing conditions. Moreover, its contribution of $\sim 30\%$ in the overall signal is not sensitive to environmental change (reduction or oxidation), strongly suggesting that this is the intrinsic fluorescence dynamics of the pool of FMOs that have cysteines successfully

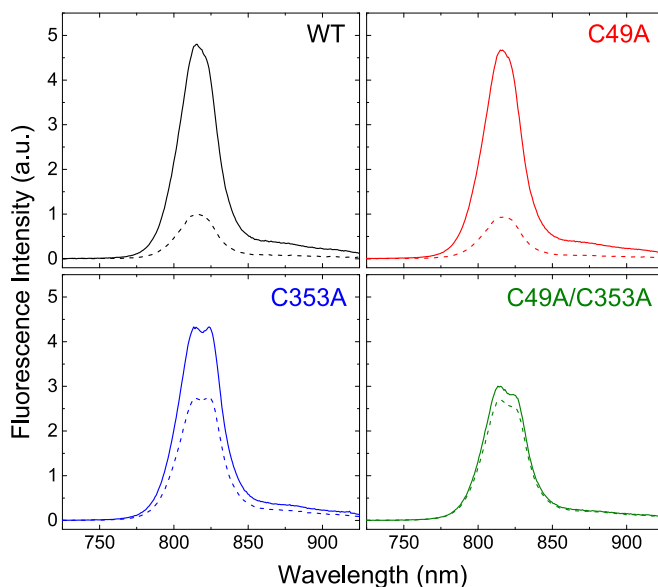


Fig. 3. Fluorescence emission response of WT FMO and the C49A, C353A, and C49A/C353A mutants to excitation at 602 nm. All samples had identical absorbance levels ($OD_{602\text{ nm}} = 0.06$) and were treated with the same amount of sodium dithionite (final concentration: 10 mM) so that all samples could be plotted on identically scaled axes for comparison. Dotted lines, air-oxidized solution; solid lines, dithionite-reduced solution.

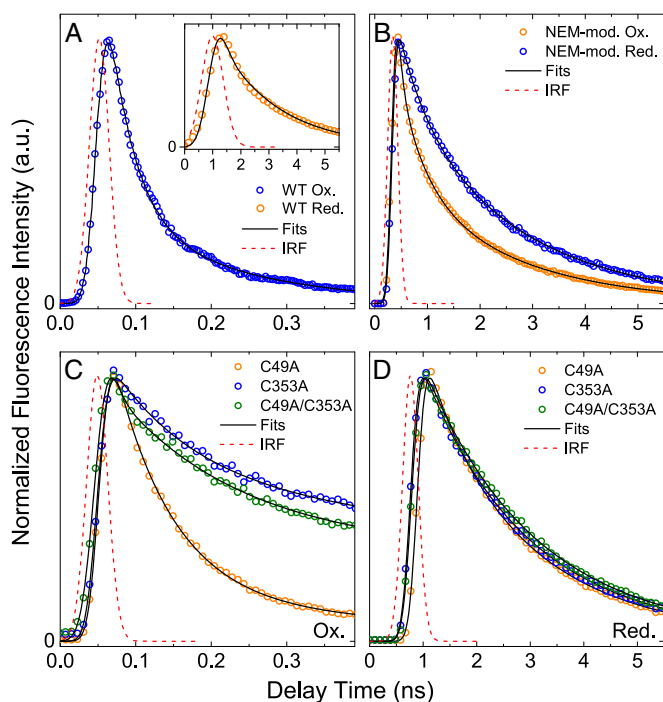


Fig. 4. TRF decay kinetics at 815 nm for WT, NEM-modified WT, and mutant FMOs after excitation at 602 nm. (A) Air-oxidized and dithionite-reduced WT protein. (B) Air-oxidized and dithionite-reduced NEM-modified WT protein. (C) Air-oxidized mutant protein. (D) Dithionite-reduced mutant protein. Note that the differences in the x-axis scales are caused by the use of different temporal windows for better resolution of data; the Gaussian approximation of each IRF is included for clarity.

labeled by NEM. Again, MS has shown that, at most, ~30% of the all FMOs are successfully NEM labeled (see above and *SI Materials and Methods*). The ~500-ps kinetic component likely derives from one or more BChl *a* molecules perturbed by the presence of the NEM moiety near their binding region within the protein.

Protein Film Voltammetry Analysis. To measure the redox potential of the redox-active groups in the WT and mutant FMO proteins, we applied protein onto a pyrolytic graphite edge (PGE) working electrode and performed protein film voltammetry using the three-electrode apparatus (reference electrode: Ag/AgCl; counter electrode: platinum wire) described previously (24–27). Fig. 5A shows the faradaic current of the unmodified FMO protein at pH 7.4 when the potential is linearly scanned from –100 mV to –400 mV (potential converted to NHE) and back again. After baseline subtraction, reductive and oxidative peaks are observed. The average midpoint potential is –272 mV vs. NHE at pH 7.4. In addition, the stoichiometric number of electrons in the process,

n , was calculated by analyzing the FWHM of the reductive and oxidative peaks, respectively (28). At pH 7.4, the FWHM is 71 mV, representing an n value of 1.28. The average FWHM for WT FMO across all pH values measured is 69 mV, representing an n value of 1.32.

Additionally, the midpoint potential of the redox species in the WT FMO protein is dependent on solution pH (Fig. 5B). This plot is linear across four to five pH units, with nonlinear tailing occurring only at pH values below 3.0 and above 9.0. The slope of this pH dependence in the linear region is –52 mV per pH unit, which, coupled with the $n \sim 1$ value described above, indicates a 1:1 proton-coupled electron transfer (PCET) mechanism for the redox-active species (29).

Similar electrochemical profiles could not be observed in any of the three cysteine mutants, likely indicating that the electrochemical activity of the protein is abolished upon cysteine mutation. It is unlikely the cysteine mutations would alter proper protein adsorption to the electrode surface because the solved crystal structure of the C49A/C353A double mutant (PDB ID code 5H8Z) shows no obvious structural changes to the exterior of the protein (14).

EPR. A 1:1 PCET-type mechanism of redox transformation is a curious finding for cysteines acting alone with no other cofactors. A possible explanation for this type of mechanism would be the formation of a thiyl radical. We propose that in the transition from reducing to oxidizing conditions a cysteine thiol in the FMO protein may lose a proton and an electron to an oxidizing agent to become a thiyl radical, which should be detectable via EPR. In the 1994 paper first describing the FMO redox effect (12), EPR indicated an organic radical singlet centered at $g = 2.001$. This signature is present in oxidizing conditions but disappears in reducing conditions. We have repeated these measurements in oxidizing conditions for the WT FMO protein and the three mutants. The resulting spectra (Fig. 6) indicate that the organic radical seen in the WT protein effectively disappears upon mutation of either or both cysteine residue(s). This EPR signature is consistent with previously published spectra of thiyl radicals (30–33).

Discussion

Cysteines Play a More Important Role in Energy Transfer Through the FMO Protein than Previously Thought. In this study we have revisited the molecular source of the FMO protein's redox-dependent modulation of energy transfer. An initial MS analysis of the protein nominated the cysteine residues for further study. Cysteine modification with NEM resulted in a protein sample with altered absorption and fluorescence properties. Additionally, a 1:1 PCET transformation was electrochemically detected at a potential of –272 mV vs. the NHE at the physiological pH of 7.4. Individual and tandem mutation of the cysteine residues provided further evidence for their involvement with redox cycling in the protein. The fluorescence-quenching effect is attenuated in the C353A single mutant and is abolished in the C49A/C353A

Table 1. TRF spectral-kinetic component lifetimes (τ_n) and contribution to the overall fit (A_n)

Parameter	WT		WT-NEM		C49A		C353A		C49A/C353A	
	Ox.	Red.	Ox.	Red.	Ox.	Red.	Ox.	Red.	Ox.	Red.
A_1	1	–	0.446	–	0.893	–	0.478	–	0.478	–
τ_1 , ps	65	–	81.5	–	79.2	–	114	–	114	–
A_2	–	–	0.285	0.306	0.107	0.337	0.523	0.668	–	0.668
τ_2 , ps	–	–	555	554	691	926	1,780	1,640	–	1,640
A_3	–	1	0.269	0.694	–	0.663	–	0.332	0.523	0.332
τ_3 , ps	–	2,200	2,220	2,270	–	2,310	–	3,020	2,650	3,560

Ox., oxidized; Red., reduced.

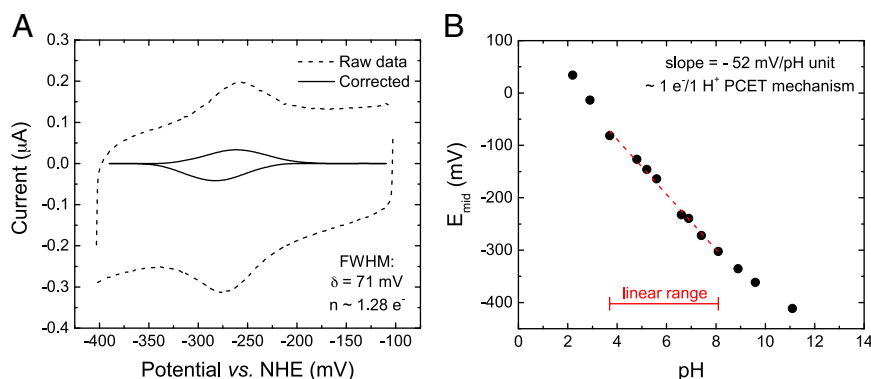


Fig. 5. Protein film voltammetry (cyclic voltammetry) of WT FMO protein adsorbed onto a PGE electrode. (A) Voltammogram showing the raw faradaic (dotted line) and baseline-corrected (solid line) current at pH 7.4. (B) Dependence of midpoint potential on pH.

double mutant. Electrochemical signatures similar to the WT could not be observed in any of the three mutants. Finally, EPR shows that a thyl radical signature present in the oxidized protein disappears upon cysteine mutation. Interestingly, the C49A mutant behaves similarly to the WT in terms of its fluorescence activity but lacks electrochemical and EPR response; although C49 and C353 are situated distantly from each other, these two residues may exert some cooperative effect on one another. Our recent determination of the C49A/C353A mutant's 3D structure via X-ray crystallography (PDB code 5H8Z) shows no evidence for secondary effects of the mutations on the structure of the protein or orientation of the pigments within their binding pockets (14). Therefore, the fluorescence, electrochemical, and EPR responses of the mutants seem to be genuinely tied to the presence of protein thiol groups.

Because excitations are delocalized within the FMO protein among its various pigments, there are many possible paths of energy transfer through the complex, with some paths being more favorable than others (19, 34–37). A recent report modeled several favorable paths for energy flow through the complex in silico, indicating that BChls 2 and 4 contribute most strongly to the final steps of energy transfer to the lowest-energy BChl *a*, BChl 3 (38). From a regulatory standpoint, it is logical for regulatory species to be positioned near two low-energy pigments (i.e., BChls 2 and 3). The mutagenesis of the cysteine residues near BChls likely changes the electrostatic environments of the pigment-binding pockets, in turn altering the observed fluorescence lifetimes of the final energy acceptors. Compelling evidence for electrostatic effects taking a role comes from the TRF experiments, which show the appearance of a new intermediate decay component in the 1-ns regime although there are no large-scale changes in protein structure upon cysteine mutation (14).

Conservation of Cysteines Across FMO and Other Antenna Complexes.

The regions surrounding the two cysteines are highly conserved across GSBs (which all contain FMO) and *Chloracidobacterium* (*Cab.*) *thermophilum* (the only outgroup known to contain the FMO protein) (Fig. 7). Cys353 is retained among all members, but Cys49 is conserved only among the closely related members of the family Chlorobiaceae (containing the genera *Chlorobium*, *Chlorobaculum*, and *Prosthecochloris*) and genus *Chloroherpeton*. “*Candidatus* (*Ca.*) *Thermochlorobacter aerophilum*” (a GSB outgroup to the family Chlorobiaceae) and *Cab. thermophilum* (an outgroup to the whole phylum Chlorobi) contain a shifted cysteine in this region or no cysteine at all, respectively. The organisms lacking the N-terminal cysteine have the capability to grow in microaerobic conditions, conditions in which other GSBs do not thrive (39, 40). If this cysteine contributes to the repression of FMO-to-RC energy transfer in oxidizing conditions, it is logical

for a microaerobe to lose this regulation to photosynthesize better in the presence of oxygen. Indeed, a past study on *Cab. thermophilum* indicated that its FMO protein is less responsive to the addition of sodium dithionite (41). This observation provides precedence for the aforementioned cooperativity between C49 and C353 in the redox effect; with *Cab. thermophilum* FMO missing one of these cysteines, its redox effect is merely attenuated, not abolished.

Surprisingly, cysteine residues are severely underrepresented among anoxygenic photosynthetic light-harvesting complexes. Using the National Center for Biotechnology Information (NCBI) protein database, we examined the LH2 proteins from 32 unique photosynthetic purple bacteria, LH1 proteins from 38 unique purple bacteria, the B806–866 complex from 10 Chloroflexi, and the CsmA baseplate protein from 20 Chlorobi and Chloroflexi (for a list of proteins and organisms, see Table S1). The total number of proteins surveyed was 127 (some organisms contained multiple isoforms of the same antenna protein). None of the CsmA or B806–866 proteins surveyed contained any cysteine residues. Of the Proteobacteria, only five species (*Rhodovulum sulfidophilum*,

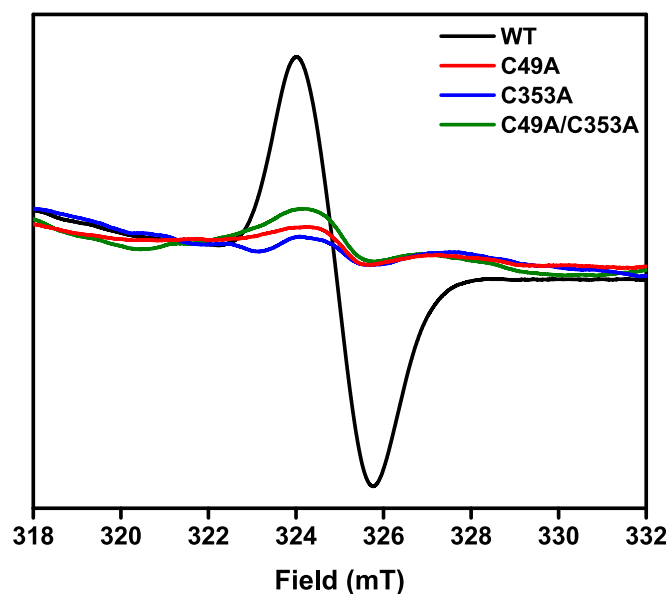


Fig. 6. Blank-corrected EPR spectra collected in oxidizing conditions at 77 K (10 30-s scans, signal-averaged) of the WT FMO protein and the three mutants. Protein was concentrated to OD_{808 nm} = 150 in 20 mM CAPS, pH 10.5 + 50% (vol/vol) glycerol.

<i>Prosthecochloris aestuarii</i> 2K	31	KGRAKV-NVPAALPELLPADCNIKIEAKPLDTQKGVVRFSTIE	72 ... 347	ARWVEHVC KGGTGQFEVLYAQ	367
<i>Pelodictyon phaeum</i>	31	KGRAKV-NVPAALPELLPADCNIKIEAKPLDQKGVVRFSTQIE	72 ... 347	ARWVEHVC KGGTGQFEVLYAQ	367
<i>Chlorobaculum parvum</i> NCIB 8327	31	KARAKV-NVPEASPLLEPADCNVKLNVPKLPDPAKGFVRFSAVIE	72 ... 345	ARWVEHVC KGGVGGQFEVLYAQ	365
<i>Chlorobaculum tepidum</i> TLS	31	KARAKV-NAPEASPLLEPADCNVKLNVPKLPDPAKGFVRFSAVIE	72 ... 346	ARWVEHVC KGGVGGQFEI LYAQ	366
<i>Chlorobium ferrooxidans</i> DSM 13031	31	KGRAKV-NVPEALPELLPADCNIKI NVKPLDPAKGFVRFSAVIE	72 ... 346	ARWVEHVC KGGTGQFEVLYAQ	366
<i>Chlorobium limicola</i> DSM 245	31	KGRAKV-NVPEASPLLEPADCNVKI NVKPLDPAKGFVRFSAVIE	72 ... 346	ARWVEHVC KGGTGQFEVLYAQ	366
<i>Chlorobium luteolum</i> DSM 273	31	KARAKV-NVPEALPELLPADCNVKI NVKPLDPAKGFVRFSAVIE	72 ... 346	ARWVEHVC KGGTGQFEVLYAQ	366
<i>Chlorobium phaeobacteroides</i> DSM 266	31	KGRAKV-NVPEASPLLEPADCNVKI NVKPLDPAKGFVRFSAVIE	72 ... 346	ARWVEHVC KGGTGQFEVLYAQ	366
<i>Chlorobium phaeovibrioides</i> DSM 265	31	KARAKV-NVPEALPELLPADCNVKI NVKPLDPAKGFVRFSAVIE	72 ... 346	ARWVEHVC KGGTGQFEVLYAQ	366
<i>Chloroherpeton thalassium</i> ATCC 35110	31	KGRANI-NVPEALPELLPADCNIKIEAKPLDQKGVVRFSTQIE	72 ... 350	KARWAEHVC KGGTGQFEI LYAQ	370
"Ca. Thermochlorobacter aerophilum"	31	KARATI-NATPAI PLLPTDLNLIKAKPKIGSNKDVWRISCLIE	72 ... 348	AKWVEHVC KGGTGQFEVLYAQ	368
<i>Chloracidobacterium thermophilum</i>	23	RAEARISNVPSASPLLPIDGELKLEAKKIE--DDVRLTFFFGQ	63 ... 346	KAWAEGIC KGSYS PFDIFFG-	365
		: * : * : * * * * * : : : : * : : . * * : : :		* * : * * * . * : : : .	

Fig. 7. Alignments of the FMO protein N-terminal and C-terminal regions from various members of the GSB phylum Chlorobi and the chlorophototrophic Acidobacterium *Chloracidobacterium thermophilum*. The alignment was constructed using Clustal Omega (www.ebi.ac.uk/Tools/msa/clustalo/). The sequence from "Ca. Thermochlorobacter aerophilum" was provided by Donald Bryant of The Pennsylvania State University, State College, PA (40). The arrows indicate conserved positions 49 and 353; cysteines are colored red.

Rhodovibrio salinarum, *Bradyrhizobium* sp. BTAi1, *Salinarimonas rosea*, and *Pseudohalialia rubra*) contained one or two cysteines in their LH2 α -polypeptide, and only one (*Bradyrhizobium* sp BTAi1) contained a cysteine in its LH2 β -polypeptide. None of the Proteobacteria contained any cysteines their LH1 α - or β -polypeptides. In the case of the photosynthetic Proteobacteria, the cysteine-containing LH2 proteins come from marine aerobes (*Rhodovulum*, *Rhodovibrio*, and *Pseudohalialia*) or green plant symbionts (*Salinarimonas* and *Bradyrhizobium*). These organisms are capable of heterotrophy and may be inclined to decrease, but not stop, photosynthetic output in aerobic conditions. Most photosynthetic Proteobacteria in general have a well-described genetic repression system to halt photosynthesis in aerobic conditions at the transcription level (42, 43); therefore a future direction would be to determine the presence or absence of such a system in the above-mentioned Proteobacteria.

A Cysteine–BChl Photochemistry Mechanism. The use of sodium dithionite in our experiments likely represents ideal reduction of the protein complex. Although sodium dithionite is an excellent industrial low-potential chemical reductant, it is not a reductant found in biology, in part because of its instability in trace amounts of water (44, 45). Therefore it is not the naturally acting reductant within the cell in vivo. A previous report from our group maintained that other reductants such as sodium borohydride and various sulfur-based reductants did not have an appreciable effect on FMO fluorescence (12). We revisited this statement, retesting the ability of other reductants (including more sulfur-based chemicals than before) to elicit optical changes in the protein, possibly illuminating its natural, endogenous reductant. The results (Fig. S4) indicate that many reductants do indeed have the ability to increase the fluorescence emission of the FMO protein, although sodium dithionite is the most effective. The best physiologically relevant reductants are reduced glutathione and sulfide, each nearly doubling the fluorescence intensity of the FMO protein. Glutathione is a compelling candidate for endogenous reductant because it has known radical activity, is present in micromolar concentrations in GSBs, and is sensitive to dissolved oxygen concentration (46, 47). Even small changes in the quenching activity of the protein are likely to result in large-scale metabolic changes. Therefore, we see this quenching mechanism as a photosynthetic "volume knob" rather than an "on/off switch."

Our current mechanistic interpretation of the data is that the redox-modulation process is an electron transfer/recombination event between a thiyl radical and excited BChl *a* that de-excites the BChl *a* (Fig. 8). In this mechanism, a thiyl radical in close proximity to an excited BChl *a* becomes a good oxidizing agent, with an excited-state electron-transfer reaction resulting in a neutral thiol (or thiolate) and a BChl *a* radical cation. The BChl

a radical cation, now a good oxidizing agent, abstracts one electron from the thiol (or thiolate), regenerating the thiyl radical and BChl *a*, now in the ground state. The excitation energy the BChl *a* originally possessed is therefore released as heat. Dithionite may be an unusually good reducing agent for the cysteine thiyl radical because it itself is in equilibrium with the [SO₂]⁻ radical anion in solution (44), affording a substrate for radical termination.

Programming a Similar Mechanism into Other Light-Harvesting Antennas. Our proposed mechanism can be envisioned as a tool for the construction of bio-inspired light-harvesting antennas or for the redesign of natural light-harvesting antennas. As an example, we examined the X-ray crystal structure (PDB code 1KZU) for the LH2 antenna complex from *Rhodoblastus acidophilus* (formerly *Rhodospseudomonas acidophila*) strain 10050. In this structure, W40 of the β -polypeptide (Puc3B) coordinates within 6 Å of the C-3 acetyl group of a B850 ring BChl *a*. In silico W40C mutagenesis predicts that the resultant cysteine will coordinate to the BChl *a* in a geometry similar to that of the cysteines from FMO (Fig. S5). In situations where energy-transfer attenuation is desired in response to changing oxygen levels, the simplicity of the cysteine–BChl interaction is an attractive option for protein engineering. An example situation in which this mechanism may be warranted would be modification of potential photosynthetic nitrogen-fixing crop symbionts (i.e., anoxygenic purple bacteria such as *Salinarimonas* and *Bradyrhizobium*) to

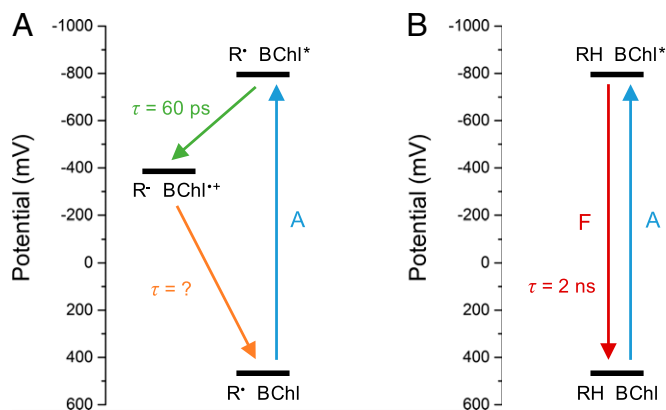


Fig. 8. Proposed electron transfer/recombination mechanism for de-excitation of BChl pigments near thiyl radicals. The y-axis scale relates to the potential of the BChl *a* species. (A) Oxidizing conditions. (B) Reducing conditions. A, absorption; F, fluorescence; R, redox-active group.

allow them to grow more efficaciously in aerobic conditions, providing essential nitrogen to the host plant. Another example would be using the cysteines to modulate the photosynthetic rate in cyanobacterial or algal biofuel cultures to control their growth rate better and thus maximize the output of the desired fuel (e.g., oil, hydrogen, and others).

Conclusion

We conclude that the cysteine-dependent excitation-quenching mechanism in the FMO protein is previously unreported in the field of photosynthesis. The FMO protein itself is unique among photosynthetic antennas in that it does not contain photoprotective carotenoids, which normally quench BChl *a* triplet states and prevent singlet oxygen sensitization. With evidence emerging that the energy level of the triplet-excited state of the FMO protein is too low to sensitize singlet oxygen (23), it is appropriate to ask why the FMO protein needs a quenching mechanism in the first place. The answer likely lies in the susceptibility of the RC to oxidative damage in the presence of oxygen. The FMO protein's redox-dependent quenching mechanism serves not to protect itself from damage but to protect the RC from receiving excitations in oxidizing conditions.

Materials and Methods

A detailed description of the materials and methods is given in *SI Materials and Methods*. The GSB *Cba. tepidum* was grown and its FMO protein was isolated as previously described (16, 48, 49), except that 20 mM CAPS (*N*-cyclohexyl-3-aminopropanesulfonic acid) buffer, pH 10.5 was substituted for Tris-HCl buffer in all chromatography steps. Oxidized FMO was used as purified in laboratory atmosphere, whereas reduced FMO was treated with 10 mM sodium dithionite in an anaerobic chamber. Three mutants of the FMO protein, C49A, C353A, and the double mutant C49A/C353A, were constructed and purified using a previously described method (14, 50). All oligonucleotides used in the construction of the mutants are provided in Table S2. For modification with NEM, 15 μ g of WT FMO protein was reduced with 10 mM sodium dithionite and treated with 10 mM final concentration of NEM in the dark for 2 h.

All protein samples for MS were precipitated with acetone, trypsin digested, peptide purified, and injected into an Ultimate 3000 Nano LC

system (Thermo Scientific Dionex) equipped with a Michrom Magic C-18 UPLC column (51). Fragments were analyzed in a Q-Exactive Plus Orbitrap mass spectrometer (Thermo Scientific). Modified peptides were identified from their accurate masses of precursor ion (MS1) spectra and product ion (MS2) spectra by either searching the NCBI database using Mascot (Matrix Science) or sequencing de novo using PEAKS 7.0 (Bioinformatics Solutions, Inc.) (18). Quantitative information about the level of chemical modification in each set of tryptic peptides was obtained from the precursor ion intensities of the peptides of interest and was compared among all samples.

Steady-state absorption spectroscopy was performed in a UV-1800 UV/Vis/NIR spectrophotometer (Shimadzu Corp. USA). Steady-state fluorescence experiments were performed using a NanoLog Spectrofluorometer (Horiba Scientific) equipped with a Vis-NIR grating and CCD detector, exciting at 602 nm. When required, samples [in 2:3 (vol:vol) buffer:glycerol] were cooled to 77 K in an Optistat DN liquid nitrogen cryostat (Oxford Instruments). TRF measurements were carried out using the laser system and universal streak camera setup described in detail previously (52), exciting at 602 nm. The spectra were cleared from noise and globally fit using the program ASUfit (13).

Protein film voltammetry was performed in an anaerobic chamber using a PGE working electrode, Ag/AgCl reference electrode, and platinum counter electrode. FMO protein was adsorbed to the working electrode surface, all electrodes were submerged in a mixed buffer electrolyte system, and cyclic voltammetry was performed with a Model 600 Series Electrochemical Analyzer workstation (CH Instruments, Inc.). All data were baseline corrected and analyzed with the program SOAS (53).

EPR was performed using a JEOL JES-FA X-BAND (9.2 GHz) or Bruker EMX-PLUS (9.2 GHz) EPR spectrometer at 77 K with quartz sample tubes. Protein was concentrated to OD_{808 nm} = 150 in 200 μ l in 50:50 (vol/vol) 20 mM CAPS buffer, pH 10.5, and glycerol. Ten 30-s scans were accumulated and averaged, and the following parameters were used during the collection of the EPR spectra: amplitude, 2,000; time constant, 0.3 s; modulation width, 0.5 mT; sweep width, 7.5 mT; frequency, 9094.105 MHz; power, 1 mW.

ACKNOWLEDGMENTS. We thank Kaitlyn Faries and Prof. Dewey Holten from Washington University for assistance with steady-state fluorescence experiments. All work, except for EPR spectroscopy, was supported as part of the Photosynthetic Antenna Research Center, an Energy Frontier Research Center funded by the US Department of Energy, Office of Science, Office of Basic Energy Sciences under Award DE-SC0001035 (to R.E.B.). The purchase of the Bruker EMX-PLUS EPR spectrometer was supported by National Science Foundation Award MRI, CHE-1429711 (to L.M.M.).

- Blankenship RE (2014) *Molecular Mechanisms of Photosynthesis* (John Wiley & Sons, Ltd., Southern Gate, Chichester, West Sussex, UK), 2nd Ed.
- Nicholls DG, Ferguson S (2013) *Bioenergetics* (Elsevier Ltd., San Diego), 4th Ed.
- Falkowski PG, Raven JA (2007) *Aquatic Photosynthesis* (Princeton Univ Press, Princeton, NJ), 2nd Ed.
- Hohmann-Marriott MF, Blankenship RE (2011) Evolution of photosynthesis. *Annu Rev Plant Biol* 62:515–548.
- Hauska G, Schoedl T, Remigy H, Tsiotis G (2001) The reaction center of green sulfur bacteria(1). *Biochim Biophys Acta* 1507(1-3):260–277.
- Büttner M, et al. (1992) Photosynthetic reaction center genes in green sulfur bacteria and in photosystem 1 are related. *Proc Natl Acad Sci USA* 89(17):8135–8139.
- Orf GS, Blankenship RE (2013) Chlorosome antenna complexes from green photosynthetic bacteria. *Photosynth Res* 116(2-3):315–331.
- Vassilieva EV, et al. (2001) Electron transfer may occur in the chlorosome envelope: The CsmI and CsmJ proteins of chlorosomes are 2Fe-2S ferredoxins. *Biochemistry* 40(2):464–473.
- Oostergetel GT, van Amerongen H, Boekema EJ (2010) The chlorosome: A prototype for efficient light harvesting in photosynthesis. *Photosynth Res* 104(2-3):245–255.
- Li H, Frigaard N-U, Bryant DA (2013) [2Fe-2S] proteins in Chlorosomes: CsmI and CsmJ participate in light-dependent control of energy transfer in Chlorosomes of Chlorobaculum tepidum. *Biochemistry* 52(8):1321–1330.
- Karapetyan NV, Swarthoff T, Rijgersberg CP, Amesz J (1980) Fluorescence emission spectra of cells and subcellular preparations of a green photosynthetic bacterium. Effects of dithionite on the intensity of the emission bands. *Biochim Biophys Acta* 593(2):254–260.
- Zhou W, LoBrutto R, Lin S, Blankenship RE (1994) Redox effects on the bacteriochlorophyll *a*-containing Fenna-Matthews-Olson protein from Chlorobium tepidum. *Photosynth Res* 41(1):89–96.
- Niedzwiedzki DM, Blankenship RE (2010) Singlet and triplet excited state properties of natural chlorophylls and bacteriochlorophylls. *Photosynth Res* 106(3):227–238.
- Saer RG, et al. (2016) Perturbation of bacteriochlorophyll molecules in Fenna-Matthews-Olson protein complexes through mutagenesis of cysteine residues. *Biochim Biophys Acta Bioenergetics* 1857(9):1455–1463.
- Tronrud DE, Wen J, Gay L, Blankenship RE (2009) The structural basis for the difference in absorbance spectra for the FMO antenna protein from various green sulfur bacteria. *Photosynth Res* 100(2):79–87.
- Li Y-F, Zhou W, Blankenship RE, Allen JP (1997) Crystal structure of the bacteriochlorophyll *a* protein from Chlorobium tepidum. *J Mol Biol* 271(3):456–471.
- Han X, Aslanian A, Yates JR 3rd (2008) Mass spectrometry for proteomics. *Curr Opin Chem Biol* 12(5):483–490.
- Ma B, et al. (2003) PEAKS: Powerful software for peptide de novo sequencing by tandem mass spectrometry. *Rapid Commun Mass Spectrom* 17(20):2337–2342.
- Milder MTW, Brüggemann B, van Grondelle R, Herek JL (2010) Revisiting the optical properties of the FMO protein. *Photosynth Res* 104(2-3):257–274.
- Hill BG, Reily C, Oh J-Y, Johnson MS, Landar A (2009) Methods for the determination and quantification of the reactive thiol proteome. *Free Radic Biol Med* 47(6):675–683.
- Rogers LK, Leinweber BL, Smith CV (2006) Detection of reversible protein thiol modifications in tissues. *Anal Biochem* 358(2):171–184.
- Liu Q, Levy EJ, Chirico WJ (1996) N-Ethylmaleimide inactivates a nucleotide-free Hsp70 molecular chaperone. *J Biol Chem* 271(47):29937–29944.
- Orf GS, Niedzwiedzki DM, Blankenship RE (2014) Intensity dependence of the excited state lifetimes and triplet conversion yield in the Fenna-Matthews-Olson antenna protein. *J Phys Chem B* 118(8):2058–2069.
- Hwang HJ, Ang M, Lu Y (2004) Determination of reduction potential of an engineered Cu(A) azurin by cyclic voltammetry and spectrochemical titrations. *J Biol Inorg Chem* 9(4):489–494.
- Johnson DL, Maxwell CJ, Losic D, Shapter JG, Martin LL (2002) The influence of promoter and of electrode material on the cyclic voltammetry of Pisum sativum plastocyanin. *Bioelectrochemistry* 58(2):137–147.
- Johnson D, Norman S, Tuckey RC, Martin LL (2003) Electrochemical behaviour of human adrenodoxin on a pyrolytic graphite electrode. *Bioelectrochemistry* 59(1-2):41–47.
- Armstrong FA, Butt JN, Sucheta A (1993) Voltammetric studies of redox-active centers in metalloproteins adsorbed on electrodes. *Methods Enzymol* 227:479–500.
- Léger C, et al. (2003) Enzyme electrokinetics: Using protein film voltammetry to investigate redox enzymes and their mechanisms. *Biochemistry* 42(29):8653–8662.
- Léger C, et al. (2001) Enzyme electrokinetics: Energetics of succinate oxidation by fumarate reductase and succinate dehydrogenase. *Biochemistry* 40(37):11234–11245.
- Salgado MT, Ramasamy S, Tsuneshige A, Manoharan PT, Rifkind JM (2011) A new paramagnetic intermediate formed during the reaction of nitrite with deoxyhemoglobin. *J Am Chem Soc* 133(33):13010–13022.
- Lassmann G, et al. (2003) Protein thyl radicals in disordered systems: A comparative EPR study at low temperature. *Phys Chem Chem Phys* 5(11):2442–2453.

32. Sevilla MD, Yan MY, Becker D (1988) Thiol peroxy radical formation from the reaction of cysteine thiyl radical with molecular oxygen: An ESR investigation. *Biochem Biophys Res Commun* 155(1):405–410.
33. Licht S, Gerfen GJ, Stubbe J (1996) Thiyl radicals in ribonucleotide reductases. *Science* 271(5248):477–481.
34. Engel GS, et al. (2007) Evidence for wavelike energy transfer through quantum coherence in photosynthetic systems. *Nature* 446(7137):782–786.
35. Fidler AF, Caram JR, Hayes D, Engel GS (2012) Towards a coherent picture of excitonic coherence in the Fenna–Matthews–Olson complex. *J Phys At Mol Opt Phys* 45(15):154013.
36. Hayes D, et al. (2010) Dynamics of electronic dephasing in the Fenna–Matthews–Olson complex. *New J Phys* 12(6):065042.
37. Panitchayangkoon G, et al. (2010) Long-lived quantum coherence in photosynthetic complexes at physiological temperature. *Proc Natl Acad Sci USA* 107(29):12766–12770.
38. Schmidt Am Busch M, Müh F, El-Amine Madjet M, Renger T (2011) The Eighth Bacteriochlorophyll Completes the Excitation Energy Funnel in the FMO Protein. *J Phys Chem Lett* 2(2):93–98.
39. Bryant DA, et al. (2007) *Candidatus Chloracidobacterium thermophilum*: An aerobic phototrophic Acidobacterium. *Science* 317(5837):523–6.
40. Liu Z, et al. (2012) ‘*Candidatus Thermochlorobacter aerophilum*’: an aerobic chlorophototrophic member of the phylum Chlorobi defined by metagenomics and metatranscriptomics. *ISME J* 6(10):1869–1882.
41. Tsukatani Y, Wen J, Blankenship RE, Bryant DA (2010) Characterization of the FMO protein from the aerobic chlorophototroph, *Candidatus Chloracidobacterium thermophilum*. *Photosynth Res* 104(2-3):201–209.
42. Masuda S, et al. (2002) Repression of photosynthesis gene expression by formation of a disulfide bond in CrtJ. *Proc Natl Acad Sci USA* 99(10):7078–7083.
43. Nickens DG, Bauer CE (1998) Analysis of the *puc* operon promoter from *Rhodobacter capsulatus*. *J Bacteriol* 180(16):4270–4277.
44. Rinker RG, Gordon TP, Mason DM, Corcoran WH (1959) The presence of the SO₂-radical ion in aqueous solutions of sodium dithionite. *J Phys Chem* 63(1):302.
45. Englander SW, Calhoun DB, Englander JJ (1987) Biochemistry without oxygen. *Anal Biochem* 161(2):300–306.
46. Madej E, Wardman P (2007) The oxidizing power of the glutathione thiyl radical as measured by its electrode potential at physiological pH. *Arch Biochem Biophys* 462(1):94–102.
47. Masip L, Veeravalli K, Georgiou G (2006) The many faces of glutathione in bacteria. *Antioxid Redox Signal* 8(5-6):753–762.
48. Gerola PD, Olson JM (1986) A new bacteriochlorophyll a-protein complex associated with chlorosomes of green sulfur bacteria. *Biochim Biophys Acta* 848(1):69–76.
49. Wen J, Zhang H, Gross ML, Blankenship RE (2011) Native electrospray mass spectrometry reveals the nature and stoichiometry of pigments in the FMO photosynthetic antenna protein. *Biochemistry* 50(17):3502–3511.
50. Frigaard N-U, Bryant DA (2001) Chromosomal gene inactivation in the green sulfur bacterium *Chlorobium tepidum* by natural transformation. *Appl Environ Microbiol* 67(6):2538–2544.
51. Zhang H, et al. (2014) Molecular mechanism of photoactivation and structural location of the cyanobacterial orange carotenoid protein. *Biochemistry* 53(1):13–19.
52. Niedzwiedzki DM, et al. (2014) Photophysical properties of the excited states of bacteriochlorophyll f in solvents and in chlorosomes. *J Phys Chem B* 118(9):2295–2305.
53. Fourmond V, et al. (2009) SOAS: A free program to analyze electrochemical data and other one-dimensional signals. *Bioelectrochemistry* 76(1-2):141–147.